Evaluation of a hybrid satellite- and NWP-based turbulent heat flux product using Tropical Atmosphere-Ocean (TAO) buoys

ChuanLi Jiang,[1] Meghan F. Cronin,[2] Kathryn A. Kelly,[3] and LuAnne Thompson[1]

Received 30 November 2004; revised 16 March 2005; accepted 1 June 2005; published 9 September 2005.

[1] Gridded hybrid turbulent heat flux fields were created by applying the state-of-the-art Coupled Ocean-Atmosphere Response Experiment (COARE) version 3.0 bulk algorithm to state variables (sea surface temperature, winds relative to currents, air temperature, and air specific humidity) derived from either numerical weather prediction (NWP) reanalysis (National Centers for Environmental Prediction–National Center for Atmospheric Research (NCEP-NCAR) reanalysis (NCEP1), NCEP reanalysis-2 (NCEP2), and 40-year European Centre for Medium-Range Weather Forecasts (ECMWF) reanalysis (ERA40)) or satellite sensors (QuikSCAT winds and Tropical Rainfall Measuring Mission (TRMM) Microwave Imager microwave sea surface temperature). The most accurate source for each state variable was determined by comparing variables to tropical Pacific Tropical Atmosphere-Ocean (TAO) buoy observations for the years 2000–2001. The selected sources were as follows: QuikSCAT for winds relative to currents, ERA40 for air temperature and specific humidity, and TRMM Microwave Imager fusion product for sea surface temperature. Errors in latent and sensible heat fluxes to state variables were analyzed. Specific humidity errors contributed the most to errors in latent heat flux (LHF). Overall, the hybrid LHF product had a bias of -5.8 W m^{-2} and a standard deviation of difference of 16.2 W m^{-2}, which is comparable to the accuracy of LHF derived from TAO measurements.

Citation: Jiang, C., M. F. Cronin, K. A. Kelly, and L. Thompson (2005), Evaluation of a hybrid satellite- and NWP-based turbulent heat flux product using Tropical Atmosphere-Ocean (TAO) buoys, *J. Geophys. Res.*, *110*, C09007, doi:10.1029/2004JC002824.

1. Introduction

[2] The air-sea heat fluxes play a critical role in climate variability, ocean circulation and heat budget modeling studies. Accurate estimates of these fluxes are an essential requirement for understanding the ocean-atmosphere coupled system. In the tropical Pacific (30°S to 30°N) latent heat flux (LHF) is the second largest term in the net air-sea heat fluxes after the shortwave radiation. The mean LHF can reach -200 W m^{-2}; hence the accuracy of LHF has become a primary issue in air-sea heat flux estimation. Numerical weather prediction (NWP) turbulent heat flux products, National Centers for Environmental Prediction–National Center for Atmospheric Research (NCEP-NCAR) reanalysis (hereafter, NCEP1) and NCEP reanalysis-2 (NCEP2) [*Kalnay et al.*, 1996], and the 40-year European Centre for Medium-Range Weather Forecasts (ECMWF) reanalysis (ERA40) [*Klinker*, 1997], are widely used in the modeling community because of their long and consistent time series and full spatial coverage, but many comparison studies with in situ measurements have shown that reanalysis heat flux errors are large and that the errors lie in both the bulk algorithms used and in the state variables themselves [e.g., *Smith et al.*, 2001; *Brunke and Zeng*, 2002; *Sun et al.*, 2003].

[3] In recent years, satellite measurements have shown their potential to provide more accurate state variables than the NWP products. The SeaWinds scatterometer on QuikSCAT, launched in mid-July 1999, provides a new opportunity to get more accurate estimates of the winds. As shown in Figure 1, mean wind speed of QuikSCAT is larger than three of the leading NWP reanalysis (NCEP1, NCEP2, and ERA40) wind speed products in the whole tropical Pacific. *Chelton et al.* [2001] have shown that both the mean and the standard deviation of the difference between QuikSCAT winds and Tropical Atmosphere-Ocean (TAO) buoy winds are less than 1.0 m s^{-1}. *Kelly et al.* [2001] showed that much of the differences between the QuikSCAT wind vectors and TAO buoy wind measure-

[1]School of Oceanography, University of Washington, Seattle, Washington, USA.
[2]NOAA Pacific Marine Environmental Laboratory, Seattle, Washington, USA.
[3]Applied Physics Laboratory, University of Washington, Seattle, Washington, USA.

0148-0227/05/2004JC002824$09.00

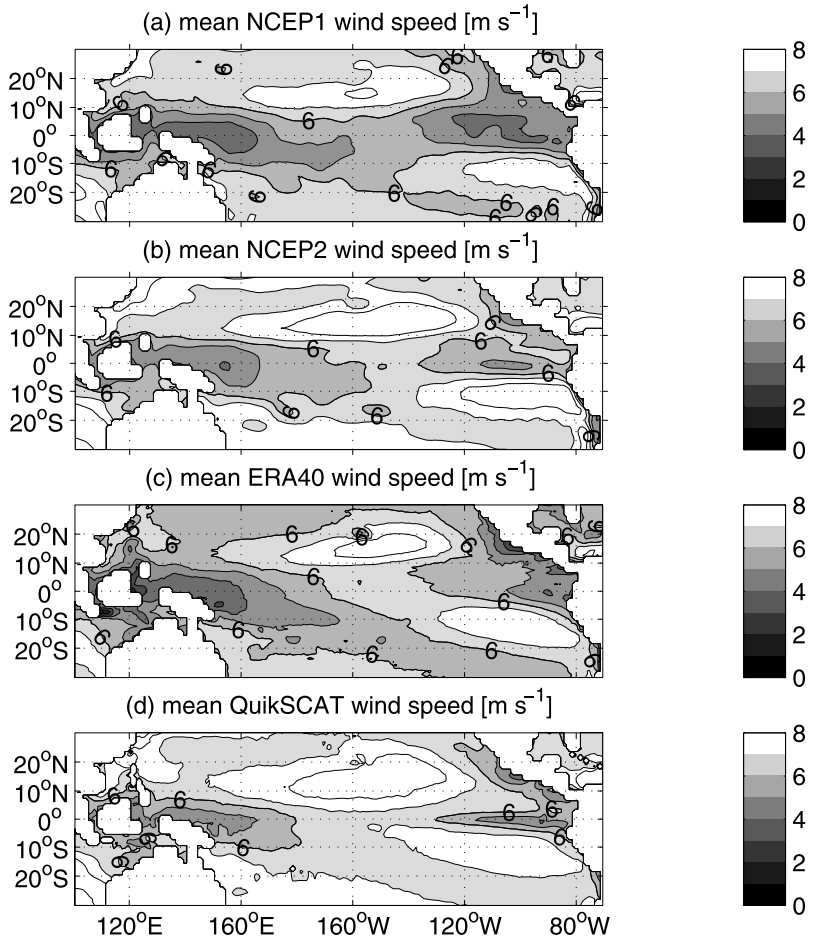

Figure 1. Two-year mean 10-m relative wind speed ($U_r = |\mathbf{U}_{air} - \mathbf{U}_s|$) map in the tropical Pacific (30°S to 30°N): (a) NCEP1, (b) NCEP2, (c) ERA40, and (d) QuikSCAT. $\mathbf{U}_s = 0$ in the NWP products. Note that QuikSCAT winds are stronger than the NWP winds.

ments could be attributed to the ocean surface currents, because the scatterometer measures winds relative to the moving ocean. In regions such as the North Equatorial Counter Current (NECC), the contribution of currents can be large relative to the winds. Although wind relative to surface currents ($U_r = |\mathbf{U}_{air} - \mathbf{U}_s|$) is a state variable for the bulk flux algorithms [*Fairall et al.*, 1996b, 2003], often currents are assumed to be zero (as in NCEP1, NCEP2, and ERA40). Such an assumption, however, could lead to significant errors in regions with strong currents. Indeed, *Bourassa et al.* [2003] attributed most of the rest of the differences to spatial/temporal mismatches in the comparison data.

[4] Near surface specific humidity and air temperature are not measurable by satellite. Some efforts have been made to estimate these two meteorological variables from other satellite measurements [e.g., *Jones et al.*, 1999; *Chou et al.*, 2003; *Clayson and Curry*, 1996], but the errors are very large. For instance, the global RMS errors of T_{air} and q_{air} estimated by *Jones et al.* [1999] are 0.72 ± 0.39°C, 0.77 ± 0.38 g kg^{-1}; the bias and daily standard deviation of q_{air} calculated by *Chou et al.* [2003] in the tropics are 1.01 g kg^{-1} and 1.11 g kg^{-1}. These errors are even larger than for NWP products in the equatorial Pacific, as will be discussed later.

[5] Usually bulk algorithms are used to estimate the turbulent heat fluxes using values of surface state variables, such as wind speed, sea surface temperature, near surface air temperature, air specific humidity, and sea level pressure [*Liu et al.*, 1979; *Smith*, 1988; *Fairall et al.*, 1996b]. For instance, LHF = $\rho_a L_v C_E U_r (q_{air} - q_s)$, where ρ_a is the density of air, L_v is the latent heat of evaporation, C_E is the turbulent coefficient of latent heat, and U_r is the 10-m wind speed relative to currents. The air specific humidity is q_{air}, and q_s is the sea specific humidity calculated from the saturation humidity q_{sat} for pure water at SST, $q_s = 0.98 q_{sat}(\mathrm{SST})$, where a factor of 0.98 is used to take into account the effect of a typical salinity of 34 psu. Several efforts have been made to compute latent heat fluxes using satellite retrievals. A sea surface turbulent flux project SEAFLUX [*Curry et al.*, 2004] gives a detailed evaluation and comparison of those satellite-based data sets. Both Hamburg Ocean Atmosphere Parameters and Fluxes from Satellite Data (HOAPS) and Japanese Ocean Flux Data Set with Use of Remote Sensing Observations (J-OFURO) provide monthly turbulent heat fluxes over the global oceans. *Chou et al.* [2003] computed the daily turbulent heat fluxes using a bulk aerodynamic algorithm with surface winds and surface air humidity from Special Sensor Microwave Imager (SSM/I), 2-m air temperature,

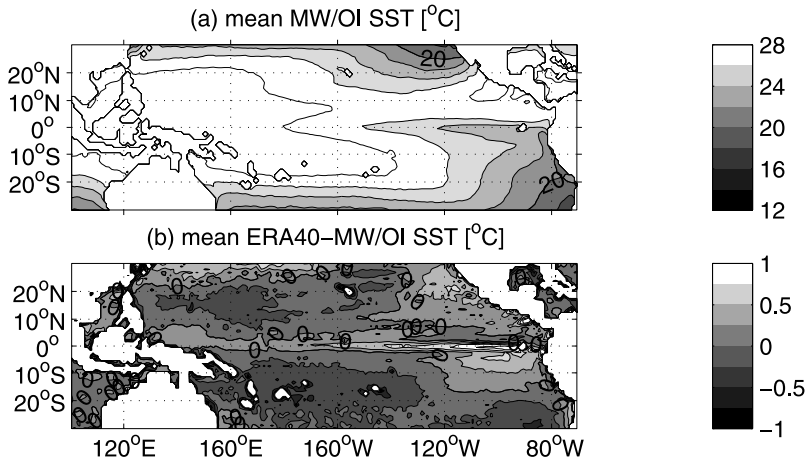

Figure 2. Two-year mean SST in the tropical Pacific (30°S to 30°N): (a) MW/OI and (b) ERA40 minus MW/OI. Compared to MW/OI SST, the NWP Reynolds SSTs are warmer in the cold tongue but colder off the equator.

and SST from the NCEP-NCAR reanalysis. *Yu et al.* [2004] used a synthesis approach, with state variables computed as a weighted average of output from NWP and satellite sources.

[6] In this paper, we use the most recent Coupled Ocean-Atmosphere Response Experiment (COARE) bulk algorithm (version 3.0) [*Fairall et al.*, 2003] to calculate turbulent heat fluxes from several sources. The COARE algorithm has been shown to be one of the least problematic of 12 bulk algorithms in calculating the turbulent heat fluxes in the tropical Pacific [*Brunke et al.*, 2003]. The COARE v3.0 bulk flux algorithm extends the maximum limit of wind speed validity from 10 m s^{-1} of COARE2.5 to 20 m s^{-1}. It improves the stability functions and eliminates a Webb correction to latent heat flux based on nearly 2800 hours of direct flux measurements [*Fairall et al.*, 2003].

[7] Our standards for comparison to choose the state variables for the turbulent heat fluxes will be the state variables from TAO buoy measurements and the fluxes calculated from TAO buoy measurements in the tropical Pacific region. A hybrid heat flux product is computed using QuikSCAT winds, microwave SST, and the best other NWP state variables based on comparisons to TAO buoy measurements. To address how much the chosen state variables affect the quality of latent heat flux products, we calculated LHF from the NWP reanalysis variables (NCEP1, NCEP2 and ERA40) using the COARE v3.0 algorithm for comparison.

[8] The paper is organized as follows. Section 2 describes all the data used in this study. Section 3 gives detailed comparisons of both the state variables and the calculated turbulent heat fluxes at the TAO buoy locations from January 2000 to December 2001. The detailed LHF map comparisons of the four heat flux estimates using the COARE v3.0 algorithm (hereafter called NCEP1C, NCEP2C, ERA40C, and hybrid) in the tropical Pacific (30°S to 30°N) for a two year time period are in section 4. In a future study, we will test how the hybrid heat flux product affect the physical processes that govern the heat budget of an OGCM in the tropical Pacific by forcing the model with the hybrid heat flux product and accompanying momentum fluxes.

2. Data

[9] The various data sets and reanalysis products are available during different times. QuikSCAT winds are available from July 1999 to present; ECMWF reanalysis (ERA40) is available from 1957 to August 2002. Therefore only two full years are analyzed in this study, from January 2000 to December 2001.

[10] To produce regularly gridded fields, the SeaWinds on QuikSCAT Level 2B winds (http://podaac.jpl.nasa.gov) from swaths are mapped into daily fields on a $1^\circ \times 1^\circ$ grid; an objective averaging scheme is used to produce maps with an approximate 4-day resolution [*Kelly et al.*, 1999]. It is worth noting that the 4-day resolution global winds map is the best temporal resolution we can get from the QuikSCAT swaths to keep the error small following [*Schlax et al.*, 2001]. For consistency with the QuikSCAT wind map temporal resolution, all other surface state variables are smoothed to 4-day temporal resolution using a similar weighting function. In other words, we compared 4-day temporal resolution turbulent heat flux products. The effect of 4-day smoothing of state variables to the turbulent heat fluxes is examined in section 3.

[11] Microwave sensors measure ocean temperature slightly deeper (about 1–2 mm) than the skin temperature, and microwave can penetrate through clouds, which the infrared advanced very high resolution radiometer (AVHRR) sensors cannot do. Therefore, even though AVHRR SST has 1-km spatial resolution, clouds decrease its effective resolution greatly. This is important, for instance, near the ITCZ. In this study, we used the fusion product from Remote Sensing Systems (RSS), which gives an optimally interpolated SST map using the Tropical Rainfall Measuring Mission (TRMM) Microwave Imager (TMI) sensor; hereafter, this product is called MW/OI SST. RSS also produces a fusion optimally interpolated product combining TMI and Advanced Microwave Scanning Radiometer for EOS (AMSR-E) sensors, but we did not use it in this

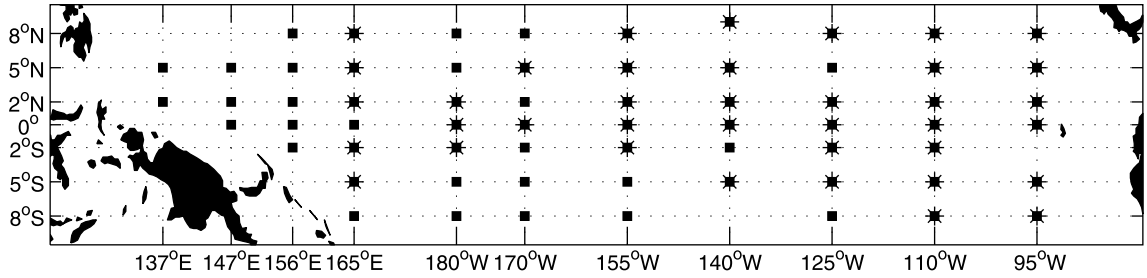

Figure 3. Locations of the 64 TAO buoys (squares and stars) for sea surface temperature, air temperature, and air specific humidity and 38 TAO buoys (stars) for wind speed and turbulent heat fluxes used in this study.

study because AMSR-E did not start until mid-2002. The 0.25° MW/OI product is smoothed to 4-day temporal resolution to be consistent with QuikSCAT. Compared to MW/OI SST, Reynolds SST is warmer in the cold tongue, but colder in the western tropical Pacific and off the equator (Figure 2).

[12] NCEP reanalysis daily state variables, such as sea surface temperature (SST), 2-m air temperature (T_{air}), 2-m air specific humidity (q_{air}), and sea level pressure (SLP) are obtained from the NCEP reanalysis Web sites. NCEP reanalysis 6-hourly zonal (u) and meridional (v) wind vectors are chosen, and the 6-hourly vector-averaged wind speeds are computed from 6-hourly wind components and then smoothed temporally to the same 4-day scalar-average as QuikSCAT for consistency. Four analyses per day (0000, 0600, 1200, and 1800 UTC) from ERA40 variables are downloaded from ECMWF. Daily means are calculated from the 6-hour snapshot values. Turbulent heat flux products from NCEP1, NCEP2, and ERA40 are also obtained directly from their Web sites for comparison.

[13] Daily resolution TAO state variables (SST, T_{air}, and relative humidity) are from NOAA's Pacific Marine Environmental Laboratory (PMEL). Hourly resolution zonal and meridional wind vectors are used to calculate the 4-m vector-averaged wind speed. A 4-day smoothing is applied to wind speed for consistency with other variables. For the evaluation, it is necessary to note the uncertainty in the TAO measurements: the accuracy of wind speed of the TAO anemometers over a range of 1–20 m s^{-1} is estimated as 0.3 m s^{-1}; the accuracy of sea surface temperature is ±0.003°C; air temperature is ±0.2°C; relative humidity is ±2.7%. Any variable whose bias is within this accuracy is considered to be as accurate as TAO. *Cronin and McPhaden* [1997] estimated an error of 10–15 W m^{-2} in latent heat flux in the warm pool of the Pacific Ocean, depending on whether the errors in the various state variables are independent or not.

3. TAO Buoy Comparison

3.1. TAO Buoy Data Description

[14] Variables from TAO/TRITON buoys with sufficiently long records (68% total data return during 2000–2001) are used as the baseline in this study. The data return criteria reduced the locations to 64 buoys for the SST, T_{air}, and q_{air} comparisons and to 38 buoys for the wind speed and turbulent heat flux comparisons (Figure 3). The TAO buoy data have been assimilated in the NWP reanalysis systems; however, the NWP reanalysis state variables still have significant errors. We use the TAO buoy in this paper to evaluate the accuracy of state variables (NCEP1, NCEP2, ERA40, QuikSCAT, and MW/OI) in the equatorial Pacific. We interpolate the NWP reanalysis and satellite products to a TAO buoy location by taking the mean of the nearby data points. If the nearest NWP or satellite grid point is within 75km of the TAO buoy, we take a simple mean as the point value; if the distance exceeds 75 km, the data at the four or six nearest grid points are weighted inversely to their distance to get the value at that TAO buoy position. TAO 4-m wind speed is converted to 10-m neutral wind speed using the COARE v3.0 algorithm.

3.2. Comparisons of State Variables

3.2.1. Wind Speed

[15] The physically correct estimates of turbulent heat fluxes require the wind speed relative to the ocean surface current U_r [e.g., *Bourassa*, 2004a, 2005], where $U_r = |\mathbf{U}_{air} - \mathbf{U}_s|$. The relative wind vectors $\mathbf{U}_r$ are what QuikSCAT measures. In this study, we subtracted zonal surface ocean currents calculated from the TOPEX/Poseidon altimeter [*Kelly et al.*, 2005] from the TAO absolute winds, and we use these relative TAO winds as the standard to evaluate wind products. We leave NCEP1, NCEP2 and ERA40 winds uncorrected because this is the way their reanalysis products are used to estimate their turbulent heat fluxes.

[16] In general, NWP reanalysis winds are weaker than TAO winds (Figure 4). The mean wind speed of NCEP1 is too low over the entire equatorial Pacific Ocean, with the largest mean negative bias of 3 m s^{-1} at 5°N 110°W. In addition, the average (over 38 buoys) bias of wind speed is −1.3 m s^{-1} for NCEP1 (Table 1). The mean wind speed of NCEP2 is much better than NCEP1 in the whole region, especially along the ITCZ (8°N), but the mean wind speed of NCEP2 is also low compared to TAO winds, with an average bias of −0.4 m s^{-1}. The wind speed of ERA40 is generally better than that of the NCEP reanalysis, particularly NCEP1, with bias of −0.5 m s^{-1}. QuikSCAT winds are quite different from the NWP reanalysis winds; there is no bias on average after TAO winds are corrected with zonal ocean currents. In the eastern equatorial Pacific QuikSCAT winds compare well with TAO winds (Figure 4), much better than either the NCEP or ERA40 reanalysis winds, but QuikSCAT winds

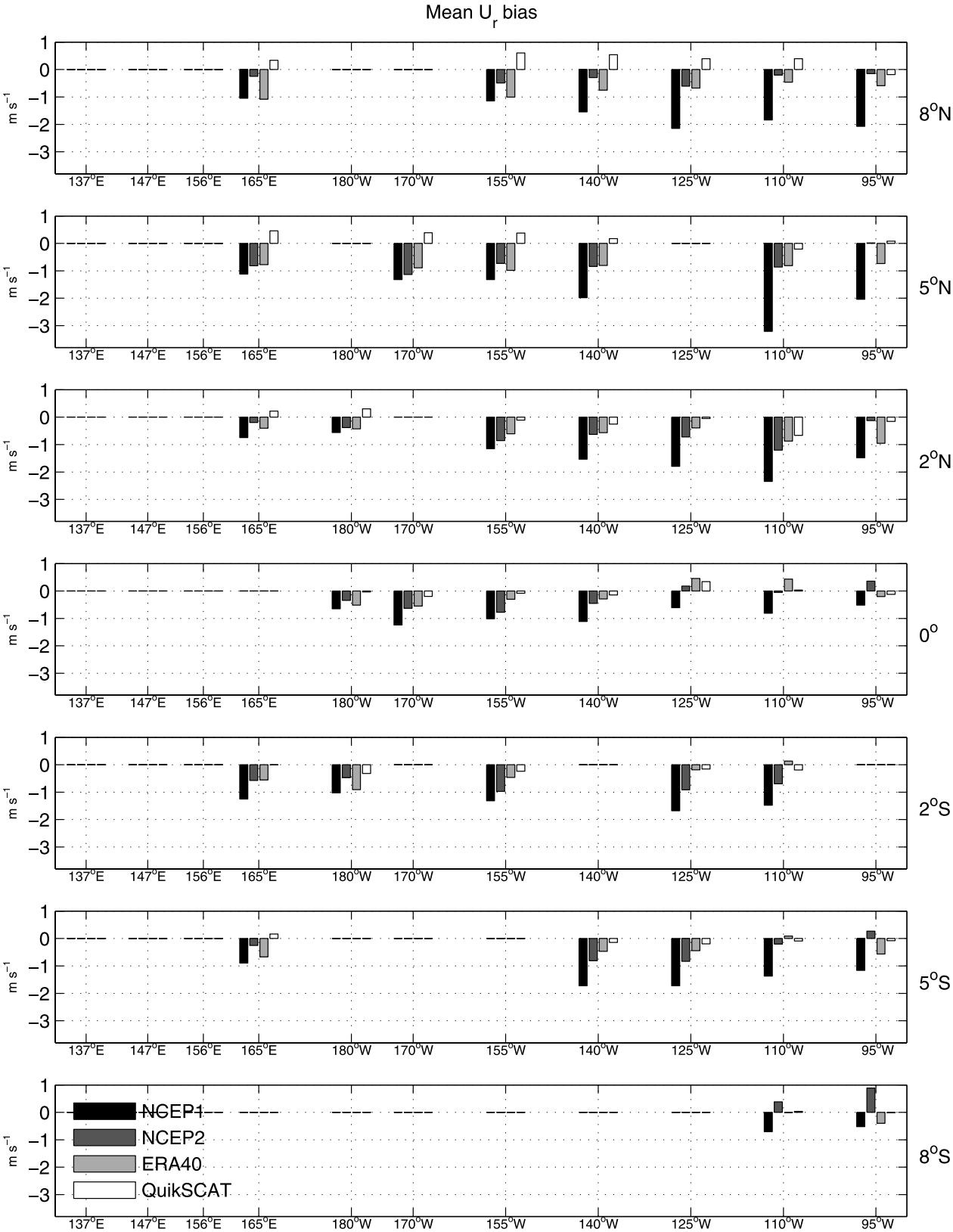

Figure 4. Bias of 10-m relative wind speed (U_r) from NCEP1, NCEP2, ERA40, and QuikSCAT relative to TAO at 38 buoys in the equatorial Pacific. The buoy at 9°N, 140°W is grouped with the 8°N buoys. Zonal ocean currents estimated from the altimeter are subtracted from TAO winds. Except for the higher than TAO winds near the ITCZ (8°N), QuikSCAT winds are much better than either the NCEP or ERA40 winds.

Table 1. Bias and Standard Deviation of the Difference of Four State Variables From NCEP1, NCEP2, ERA40, MW/OI, and QuikSCAT Relative to TAO Buoy Observations[a]

	SST, °C		T_{air}, °C		q_{air}, g kg^{-1}		U_r, m s^{-1}	
Sources	Bias	SDD	Bias	SDD	Bias	SDD	Bias	SDD
NCEP1	−0.1	0.3	−0.2	0.5	0.0	0.8	−1.3	0.9
NCEP2	−0.1	0.3	0.1	0.5	−0.4	0.8	−0.4	1.0
ERA40	0.0	0.3	−0.1	0.3	−0.0	0.5	−0.5	0.6
MW/OI	−0.1	0.3						
QuikSCAT							0.0	0.5

[a]SDD, standard deviation of the difference. Statistics of SST, T_{air}, and q_{air} are calculated from 64 buoys, and U_r is calculated from 38 buoys.

are higher than TAO winds in the western Pacific (165°E), and near the ITCZ (8°N).

[17] The histograms of wind speeds show over what speed range the wind speed errors occur for each product (TAO, QuikSCAT, ERA40, NCEP2, and NCEP1). In the eastern equatorial Pacific at 0°N 140°W (Figure 5, left panel), QuikSCAT 4-day wind speed matches TAO winds best within all wind speed ranges (3–10 m s^{-1}). The ERA40 matches TAO winds well at low wind speed, but gives too few high-wind-speed values. NCEP2 wind speeds are too low, with larger errors at high wind speeds than ERA40 winds, and NCEP1 winds are even weaker than NCEP2. Comparing to daily resolution TAO winds (Figure 5, right panel), the 4-day smoothing needed for QuikSCAT removes both low and high winds. Again both ERA40 and NCEP2 daily wind histograms match very well with TAO at low wind speeds, but have too few values at the higher speeds. NCEP1 daily winds are again clearly too weak.

[18] Near the ITCZ at 8°N 110°W (Figure 6), histograms show too few QuikSCAT values at low wind speeds (1–3 m s^{-1}) compared to TAO winds, both in the 4-day resolution (left panel) and in the daily winds (right panel). Both ERA40 and NCEP2 are missing high wind speeds, although overall, the match with TAO winds of NCEP2 is better than for ERA40. Near the ITCZ, the NECC opposes the generally easterly winds, making the scatterometer winds stronger than an anemometer wind. The higher mean wind speed of QuikSCAT near the ITCZ (shown in Figure 4) may be in part owing to an underestimate of the zonal ocean current which we used to correct TAO winds. Current corrections to the TAO anemometers were derived from the altimeter, supplemented by a mean derived from 10-m drifter data [*Kelly et al.*, 2005]. These estimates reproduce only the zonal wind differences between QuikSCAT and TAO buoy and tend to be somewhat smaller than the actual currents. The weaker ocean surface current estimate might be a factor contributing to the wind speed mismatch where ocean current and winds have opposite direction, near the ITCZ. In addition, the lack of a meridional ocean current estimate

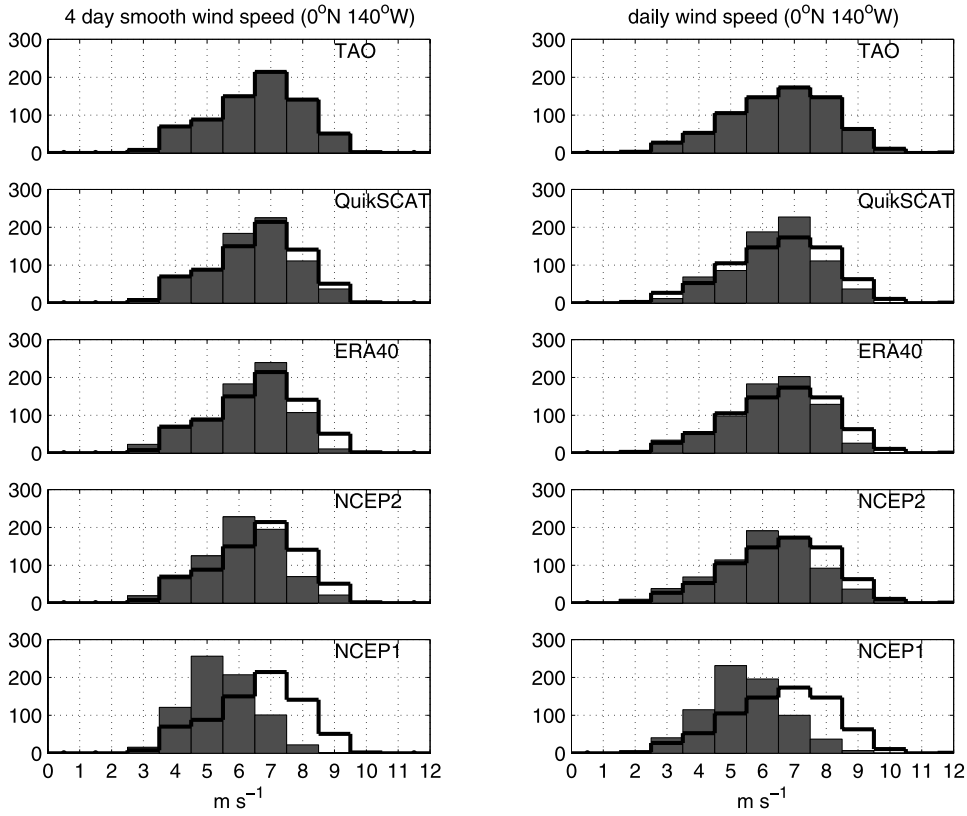

Figure 5. Histograms of 10-m wind speed (U_r) of TAO, QuikSCAT, ERA40, NCEP2, and NCEP1 (from top to bottom) at 0°N, 140°W. The left panel illustrates the 4-day smoothed wind speeds, while the right panel shows the daily wind speed histograms. Note that 4-day resolution QuikSCAT winds are used in the daily wind comparison. The thick lines are the histograms from the TAO winds.

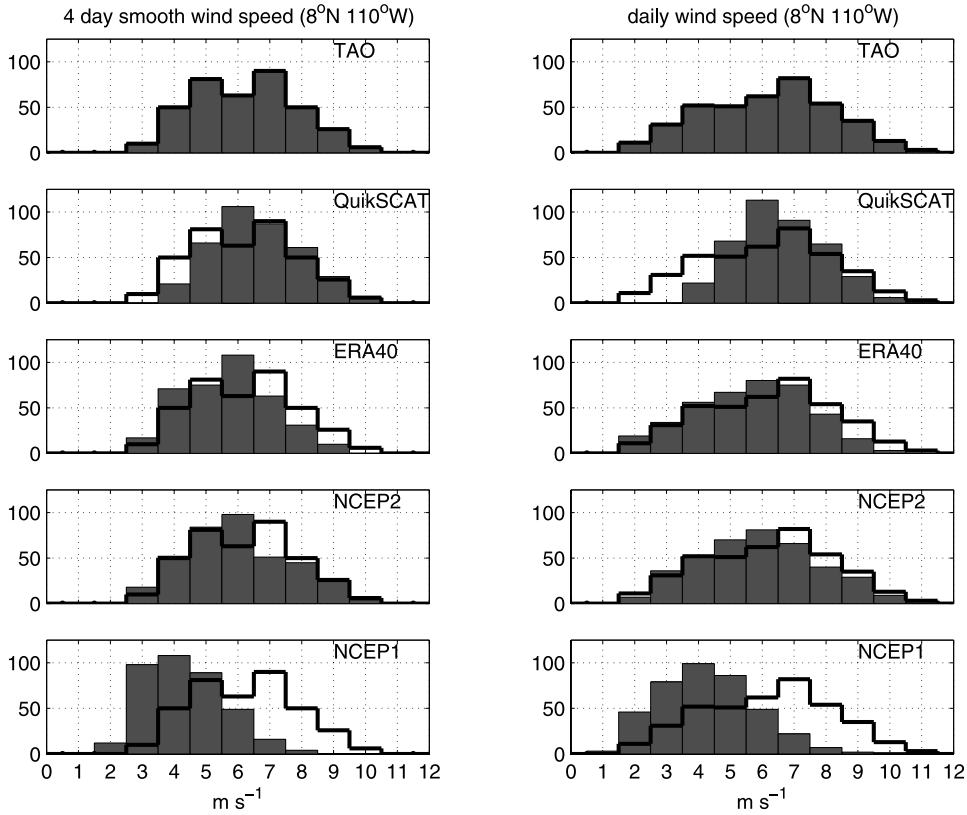

Figure 6. Same as Figure 5 but at 8°N, 110°W. Clearly, QuikSCAT winds do not match with TAO winds at low wind speed at both 4-day and daily resolution.

might be another factor in the mismatch. Or, it may be owing in part to an increase in apparent wind speed caused by precipitation effects on the ocean surface [e.g., *Stiles*, 2002; *Tournadre*, 2003; *Contreras and Plant*, 2004]. The QuikSCAT Level 2B swath winds include both the Multidimensional Histogram Rain Flag [*Huddleston*, 2000] and the Normalized Objective Function Rain Flag [*Mears*, 2000], a strict threshold is used to flag the rain-contaminated data in the mapped QuikSCAT winds [*Kelly et al.*, 1999]. Even though the strict rain flags allow some rain-contaminated data to be considered valid, the contribution of QuikSCAT rain-contaminated data to the wind speed mismatch near the ITCZ might not be significant.

3.2.2. Sea Surface Temperature

[19] Daily 1/4-degree spatial resolution MW/OI SST may give more accurate SST estimates, because microwave sensors can measure the SST through the clouds, which is an advantage over AVHRR SST, where persistent clouds exist above the ocean.

[20] Although the average bias and standard deviation of difference (SDD) of all four SST products are very close (see Table 1), the geographical comparisons of the 2-year bias (Figure 7a) and SDD (Figure 7b) of SST of NCEP1, NCEP2, ERA40, MW/OI relative to TAO show some different features. Because of the small biases in the western Pacific, only comparisons at buoys east of 155°W and within 2° the equator are shown. NCEP and ERA40 operational satellite SST products show very similar patterns to each other: too warm along the equator (0°N), but too cold just off the equator (2°S and 2°N). The bias of MW/OI SST is negative (cooler) throughout the tropical Pacific, consistent with the expected cool skin effect [*Fairall et al.*, 1996b]. The satellite MW/OI SST is nominally at 1–2-mm depth, while the TAO bulk SST is at 1-m depth. The standard deviation of MW/OI errors (Figure 7b) is smaller in the eastern equatorial ocean than that for NCEP or ERA40 SST. In the western Pacific, both NCEP and ERA40 SDDs decrease substantially, whereas the MW/OI errors are consistent in magnitude throughout the tropics, so that MW/OI random errors are larger in the western Pacific (not shown).

3.2.3. Air Specific Humidity

[21] As shown in Figure 8, ERA40 specific humidity is more accurate than those of NCEP reanalysis in the whole region; this conclusion can also be confirmed from average statistics (Table 1). Note that NCEP specific humidity is too high in the western Pacific, but too low in both the central and eastern equatorial Pacific. The NCEP2 reanalysis has an improved 2-m air specific humidity near the ITCZ, but it is worse than NCEP1 in other regions of the eastern Pacific and worse in the central Pacific. Table 1 indicates that the bias of specific humidity of NCEP2 (-0.4 g kg^{-1}) is larger than that of NCEP1, but it has the same SDD (0.8 g kg^{-1}).

3.2.4. Air Temperature

[22] ERA40 air temperature has a smaller standard deviation of difference than the NCEP reanalysis (Table 1). Averaged over the whole region, air temperature is biased

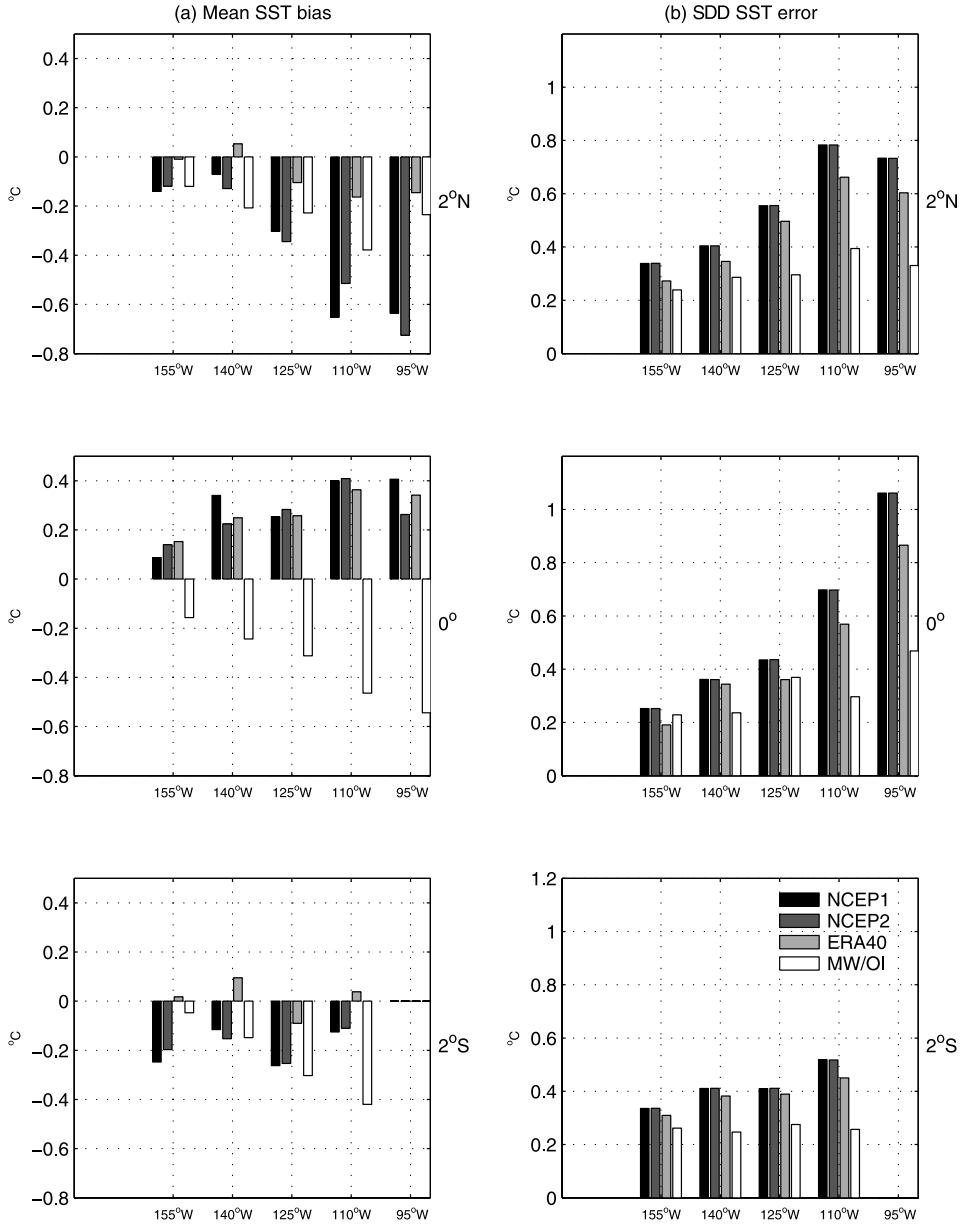

Figure 7. (a) Bias and (b) standard deviation of difference of sea surface temperature (SST) of NCEP1, NCEP2, ERA40, and MW/OI relative to TAO within 2°S to 2°N. Compared to TAO SST, NWP Reynolds SST is too warm in the cold tongue but too cold off the equator; MW/OI is consistently cold and has a smaller SDD.

low by 0.1 °C in ERA40, by 0.2 °C in NCEP1, and is biased high by 0.1 °C in NCEP2.

3.3. Errors of Turbulent Heat Fluxes to Surface State Variables

[23] To understand the accuracy of turbulent heat fluxes, we test the errors of the heat fluxes to different surface state variables. This analysis demonstrates how errors in the state variables affect errors of the turbulent heat fluxes, and gives us direction on how to choose the best state variables for our hybrid turbulent heat flux product. To test the errors of turbulent heat flux to a given variable, we used all other state variables from TAO, replacing the given variable one at a time by that from NCEP1, NCEP2, ERA40, MW/OI, or QuikSCAT. After calculating the turbulent heat flux with the COARE v3.0 algorithm with each variable, we calculated the statistics of differences of the turbulent heat fluxes from the TAO fluxes (Tables 2 and 3).

[24] The error analysis of latent heat flux to four state variables (Table 2) suggests that in order of importance the errors of air specific humidity, wind speed, and SST contribute to the errors in LHF estimation in the tropical Pacific. The error of LHF to air temperature (T_{air}) is so small that it can be neglected. The errors in LHF due to discrepancies in wind speed relative to TAO U_r show that NCEP2 winds are an improvement over NCEP1 winds. Indeed,

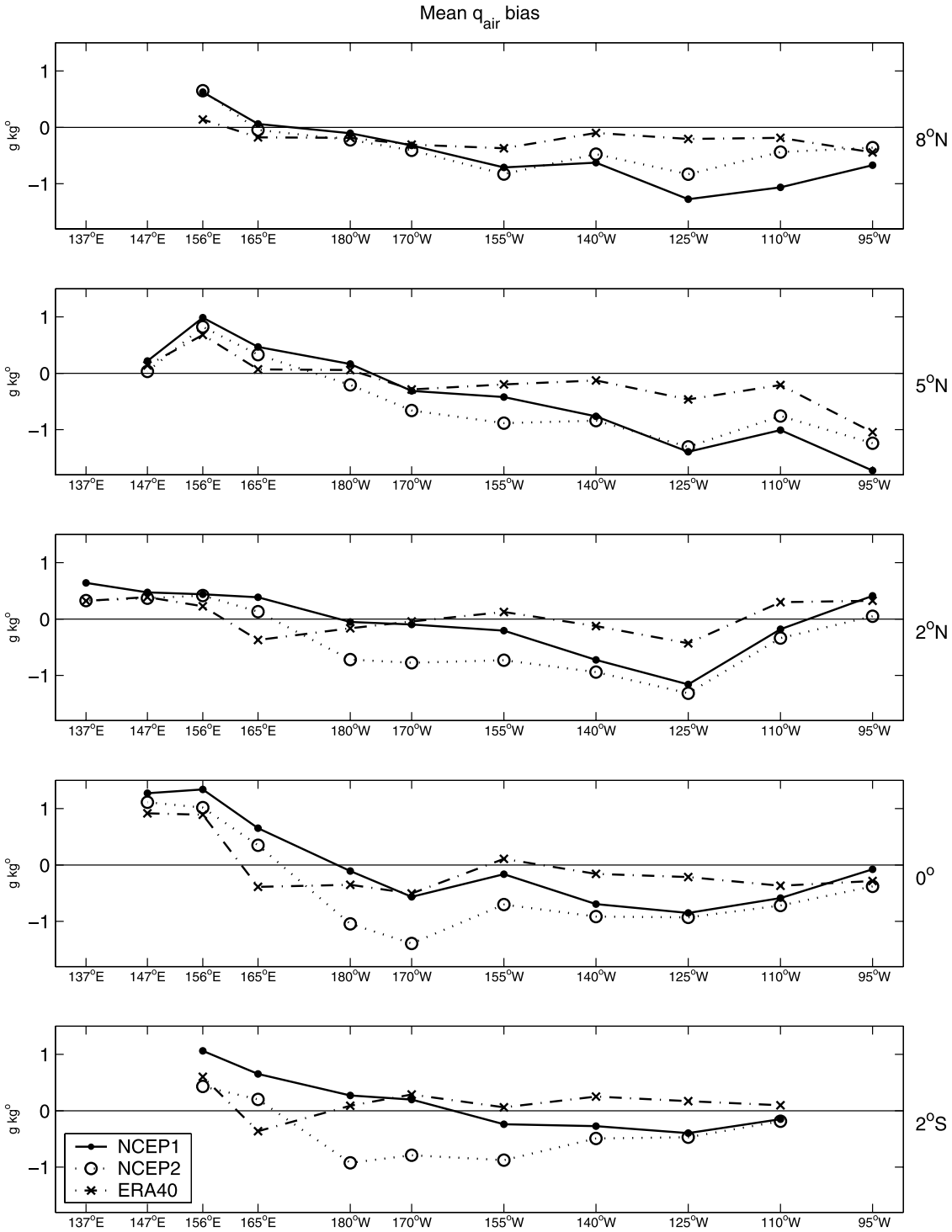

Figure 8. Bias of 2-m air specific humidity (q_{air}) of NCEP1 (solid lines), NCEP2 (dotted lines), and ERA40 (dash-dotted lines) relative to TAO at 8°N (top) to 2°S (bottom). Note that ERA40 has a more accurate q_{air} product than NCEP.

NCEP2 winds lead to the smallest bias in LHF. However, the SDD for NCEP2 winds is nearly twice as large as the SDD for QuikSCAT winds. QuikSCAT winds also have a slightly smaller bias and SDD than ERA40. For SST, the LHF errors are close for all products. ERA40 has the smallest bias, but MW/OI SST has the smallest SDD. ERA40 has the most accurate air specific humidity among the NWP products. Therefore the satellite retrievals (QuikSCAT wind, microwave SST) in this study have shown their potential to provide better state variables.

Table 2. Error of LHF to SST, T_{air}, q_{air}, and U_r[a]

	Latent Heat Flux Error Using the Given Variable Sources, W m^{-2}							
	SST, °C		T_{air}, °C		q_{air}, g kg^{-1}		U_r, m s^{-1}	
Sources	Bias	SDD	Bias	SDD	Bias	SDD	Bias	SDD
NCEP1	2.3	11.6	−0.8	1.4	−6.3	18.3	15.0	13.0
NCEP2	1.6	11.6	0.2	1.4	−13.1	18.4	2.5	13.8
ERA40	−0.5	10.4	−0.4	1.0	−4.8	11.0	4.4	8.3
MW/OI	3.7	8.5						
QuikSCAT							−4.0	6.9

[a]Values are listed as the bias and standard deviation of the difference (SDD) between each LHF estimate and the LHF from TAO observations averaged over 38 TAO buoys (see text for detailed explanation).

However, air specific humidity is not measurable from satellites; and its accuracy is a major issue in latent heat flux estimates at present.

[25] The error analysis of sensible heat flux to state variables (Table 3) indicates that the errors of air temperature, SST, and wind speed contribute to the errors in SHF estimation. The error of SHF to specific humidity is so small that it can be neglected. All products have roughly comparable errors.

3.4. Comparisons of Turbulent Heat Fluxes

[26] We calculated turbulent heat fluxes from NCEP1, NCEP2, and ERA40 state variables using the COARE v3.0 algorithm at the TAO buoy positions, which we will refer to as NCEP1C, NCEP2C, and ERA40C products respectively. In addition, we calculated a hybrid turbulent heat flux product by using QuikSCAT wind speed, MW/OI SST, and all other state variables from ERA40, which has the best T_{air} and q_{air} among the NWP products. Finally, we calculated the turbulent heat flux with all TAO surface state variables except with sea level pressure from NWP products (the error analysis suggests that the effect of sea level pressure errors is negligible in flux estimates) as a baseline to evaluate those four turbulent heat flux estimates. In the COARE v3.0 algorithm we did not include the cool-skin and warm-layer effect to correct the bulk SST to skin SST, because the hourly shortwave and longwave TAO data were not available. The SEAFLUX study [*Curry et al.*, 2004] showed that using bulk SST instead of skin SST can cause a 10% error in estimating turbulent heat fluxes, and about a 7 W m^{-2} error in the warm pool during COARE experiment [*Fairall et al.*, 1996a]. A combination of the microwave SST, infrared satellite SST, and an estimate of the diurnal cycle would be ideal to provide an accurate skin SST [*Curry et al.*, 2004].

[27] Generally, the average (over 38 TAO buoys) RMS errors of ERA40C and the hybrid LHF estimates are comparable (Table 4), and better than the NCEPC (NCEP1C and NCEP2C) fluxes, but the errors vary by region (Figure 9). The mean LHF of the hybrid estimate is best in the eastern equatorial Pacific, but in the western equatorial Pacific (165°E) and near the ITCZ (8°N), the hybrid estimate is worse than ERA40C. The reason is that the low bias of low wind speed and cold SST of ERA40 compensate for the high bias from its small air specific humidity, both in the western equatorial Pacific and near the ITCZ, while the high wind speed of QuikSCAT increases the LHF from air specific humidity even more. Overall, the LHF of the hybrid estimate is biased high (flux too large by 5.8 W m^{-2}) compared with that calculated using all TAO measurements. Similarly, the average RMS error of ERA40C and the hybrid SHF estimates are comparable, and better than the NCEPC fluxes (Table 4). Since LHF and SHF have similar statistic patterns, and SHF is much smaller in magnitude than LHF, figures for SHF are not shown.

[28] Thus far we have compared fluxes from different variables using a common bulk algorithm, COARE v3.0. To address the contribution of different algorithms to the turbulent heat fluxes, we also compared the 4-day smoothed LHF obtained directly from the NWP reanalysis (hereafter called NCEP1, NCEP2, and ERA40 heat flux products) with the TAO fluxes (Table 5). The differences between the NWP turbulent heat fluxes evaluated in Table 4 and Table 5 are the bulk algorithms used to estimate the fluxes, the temporal resolution of surface state variables input to the bulk algorithm, and the state variables used in the NWP reanalysis heat flux products. Even though the 4-day resolution of NWP surface variables lacks shorter time variability, the error of the LHF bias in the COARE v3.0 algorithm to state variables of different temporal resolution (hourly and 4-day) is shown to be negligible in the equatorial Pacific; this suggests that the COARE v3.0 algorithm is not highly nonlinear with respect to fluctuations at timescales shorter than 4 days. However, 4-day temporal resolution does lose the high-frequency variability, which can be essential in some ocean modeling studies. NWP heat flux products are calculated using the state variables from

Table 3. Same as Table 2 but for SHF

	Sensible Heat Flux Error Using the Given Variable Sources, W m^{-2}							
	SST, °C		T_{air}, °C		q_{air}, g kg^{-1}		U_r, m s^{-1}	
Sources	Bias	SDD	Bias	SDD	Bias	SDD	Bias	SDD
NCEP1	0.5	3.5	−2.7	4.6	0.0	0.0	1.0	1.1
NCEP2	0.4	3.5	0.5	4.5	0.0	0.0	0.1	1.1
ERA40	−0.3	3.1	−1.2	3.1	0.0	0.0	0.3	0.7
MW/OI	1.1	2.5						
QuikSCAT							−0.4	0.7

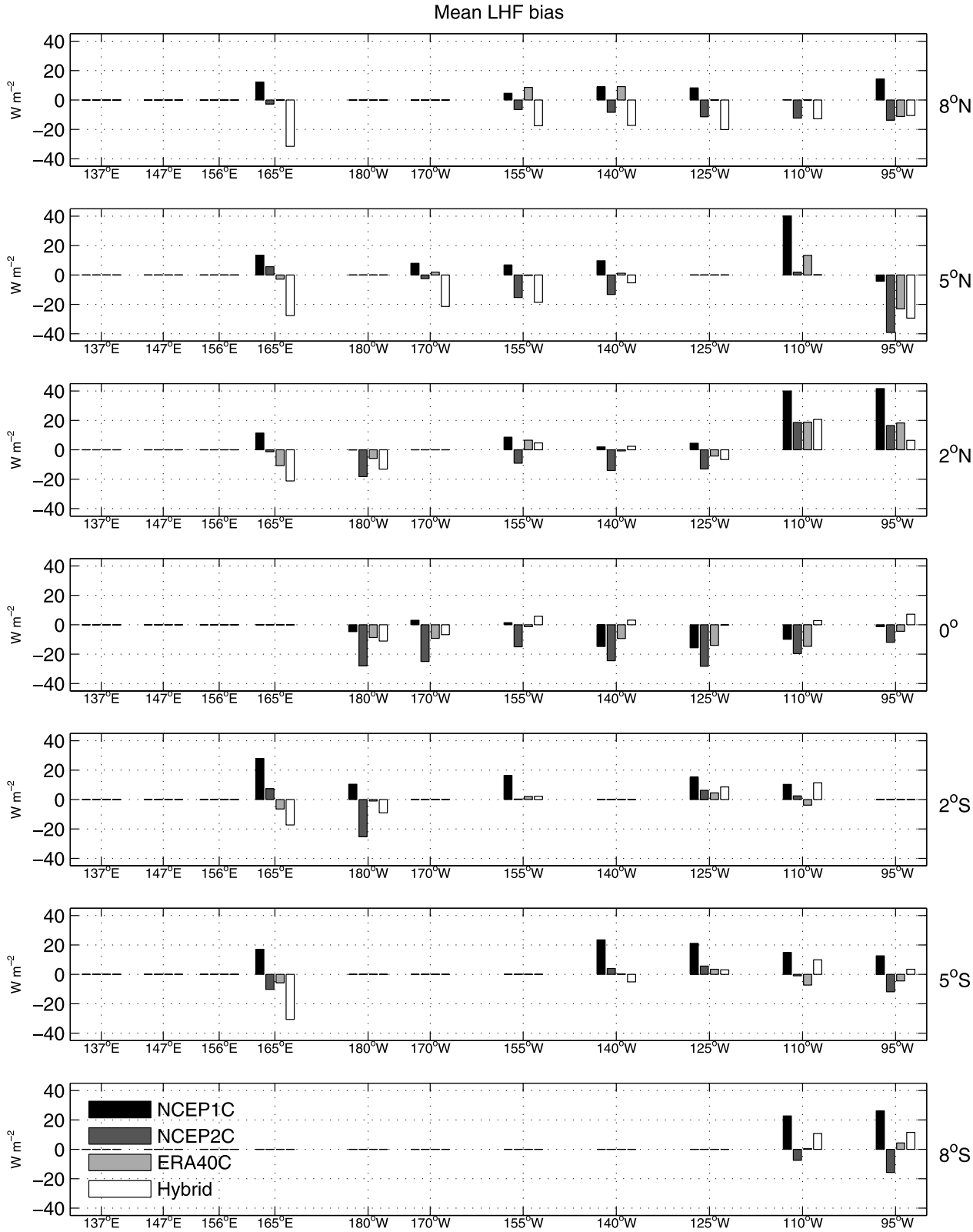

Figure 9. Same as Figure 4 but for latent heat flux. The hybrid heat flux product is the best in the eastern Pacific but too high in the western Pacific and near the ITCZ.

Table 4. Bias and SDD of Four Turbulent Heat Flux Estimates Using the COARE v3.0 Algorithm (NCEP1C, NCEP2C, ERA40C, and Hybrid) Relative to TAO[a]

	NCEP1C		NCEP2C		ERA40C		Hybrid	
Field	Bias	SDD	Bias	SDD	Bias	SDD	Bias	SDD
LHF	10.7	24.8	−8.9	26.6	−1.5	18.1	−5.8	16.2
SHF	−0.9	4.2	1.0	4.1	−1.0	3.2	−0.4	4.1

[a]Values are given in W m^{-2}. Statistics are from 38 TAO buoys.

prediction models rather than from analysis models, which suggests that state variables in NWP heat flux products lack observational constraints. Therefore the difference between the NWP turbulent heat fluxes between Table 4 and Table 5 likely results from different algorithms and different state variables. Comparing Table 5 to Table 4, we can see that the COARE 3.0a algorithm and the reanalysis state variables together changed both the bias and SDD of the turbulent heat fluxes of both ERA40 and NCEP2 relative to TAO fluxes, especially for NCEP2 latent heat flux. As we mentioned in section 1, the standard for comparison fluxes is the fluxes calculated from TAO observations with the COARE v3.0 algorithm. Relative to this standard, the ERA40 LHF product is biased high by about 13.6 W m^{-2}, but the LHF with COARE v3.0 algorithm has only a 1.5 W m^{-2} bias. The NCEP2 LHF product has a bias of about 28.6 W m^{-2} (too large), while the LHF with COARE v3.0 algorithm has a bias of only 8.9 W m^{-2}. For NCEP1, the LHF product is high by 4.7 W m^{-2}, which is closer to the TAO estimate than the fluxes using the COARE v3.0 algorithm (10.7 W m^{-2} low). Switching the bulk algorithms in NCEP2 and ERA40 reanalysis to the COARE v3.0 algorithm could give better turbulent heat flux products, especially in the tropical Pacific. The bias in the NCEP1 LHF product is relatively small, despite very weak winds, suggesting that the bulk algorithm in NCEP1 compensated for low wind speeds. In NCEP2, wind speeds are much higher, closer to observed speeds, and the bulk algorithm was not revised [*Kanamitsu et al.*, 2000], so that the higher NCEP2 winds have caused the LHF to be biased even higher.

4. Comparison of Maps in the Tropical Pacific

[29] Having compared the surface state variables and the turbulent heat fluxes at TAO buoys in section 3, we now compare maps of variables and products in the tropical Pacific. To address how the hybrid product (QuikSCAT winds, MW/OI SST, and ERA40 air temperature and air specific humidity) is different from the products estimated with NWP reanalysis variables, we produce four sets of 2-year-mean variables and turbulent heat flux maps in the tropical Pacific (30°S to 30°N) from January 2000 to December 2001.

[30] As we discussed in section 1 and section 2, the mean wind speed of NWP is smaller than the QuikSCAT winds in the whole tropical Pacific (Figure 1), and the Reynolds SST is colder than the MW/OI SST in the whole region except for the cold tongue (Figure 2).

[31] The mean LHF estimates are more different from each other off the equator than in the TAO buoy array, with the hybrid LHF about 25–50 W m^{-2} higher than ERA40C and NCEP2C estimates using the COARE v3.0 algorithm (Figure 10). The difference of LHF between the hybrid and ERA40C is probably owing to the strong wind speed of QuikSCAT (Figure 1) and the warm MW/OI SST (Figure 2); in addition, the low wind speed and cold SST in ERA40 compensate for the too low specific humidity. The NCEP1C LHF estimate is the smallest, particularly off the equator.

[32] In the NWP reanalysis heat flux products, the NCEP2 magnitude is much larger than that for either ERA40 or NCEP1 off the equator (Figure 11). Interestingly, the structure of the hybrid LHF (Figure 10d) is very similar to that of NCEP1 (Figure 11c), but with the hybrid LHF magnitude off the equator higher.

5. Discussion and Conclusion

[33] In this study point comparisons on 64 (for sea surface temperature, air temperature, and air specific humidity) and on 38 (for wind speed, and turbulent heat fluxes) TAO buoys are performed to evaluate state variables and turbulent heat fluxes. The point comparisons at the TAO buoys provided the standard for us to estimate errors in state variables and in heat fluxes. However, point comparisons cannot provide the spatial information that is important for numerical models. The spatial coverage and resolution requirement for the forcing numerical models has motivated this study and our efforts to create a hybrid turbulent heat flux product.

[34] Satellite sensors provide high-spatial-resolution data. Our QuikSCAT mapped wind product has 1° spatial resolution. The higher spatial resolution of QuikSCAT winds over that of the NWP reanalysis products (either the Gaussian grid of NCEP or the 2.5° grid for ERA40) can resolve the meridional gradient of the zonal winds, which plays a crucial role in ocean modeling studies. The MW/OI SST has a 0.25° spatial resolution. Therefore we expect that the turbulent heat flux estimates using QuikSCAT winds and MW/OI SST are more appropriate to study the heat budget in the tropical Pacific, where the balance of terms may change rapidly, particularly in the meridional direction. Another RSS MW/OI fusion SST product that combines TMI and AMSR-E temperature sensors (since June 2002) may give a more accurate SST and correspondingly accurate turbulent heat fluxes. The high spatial resolution of QuikSCAT winds are obtained by reducing temporal resolution to 4 days, which would negatively impact high-temporal-resolution studies, or long-term variability in ocean modeling. Comparisons of the histograms (Figures 5 and 6) of 2-year time series of wind speeds show that QuikSCAT winds are the best for 4-day temporal resolution and that the reduction of temporal resolution does not cause LHF biases when using the COARE v3.0 algorithm.

Table 5. Bias and SDD of NWP Turbulent Heat Fluxes (NCEP1, NCEP2, and ERA40) Relative to TAO Estimated From COARE v3.0 Algorithm[a]

	NCEP1		NCEP2		ERA40	
Field	Bias	SDD	Bias	SDD	Bias	SDD
LHF	−4.7	26.8	−28.6	32.0	−13.6	18.1
SHF	−0.9	4.6	0.9	4.4	−2.0	3.5

[a]Values are given in W m^{-2}. Statistics are from 38 TAO buoys.

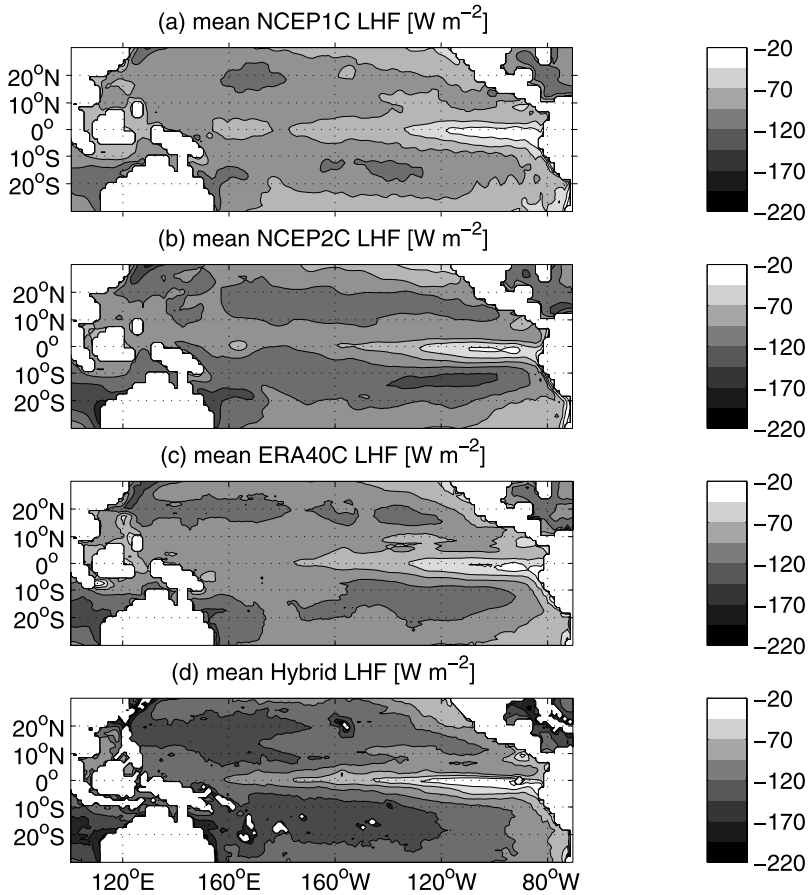

Figure 10. Two-year mean LHF estimates using the COARE v3.0 algorithm in the tropical Pacific (30°S to 30°N): (a) NCEP1C, (b) NCEP2C, (c) ERA40C, and (d) hybrid. Note that the hybrid LHF is 25–50 W m^{-2} higher than ERA40C and NCEP2C off the equator.

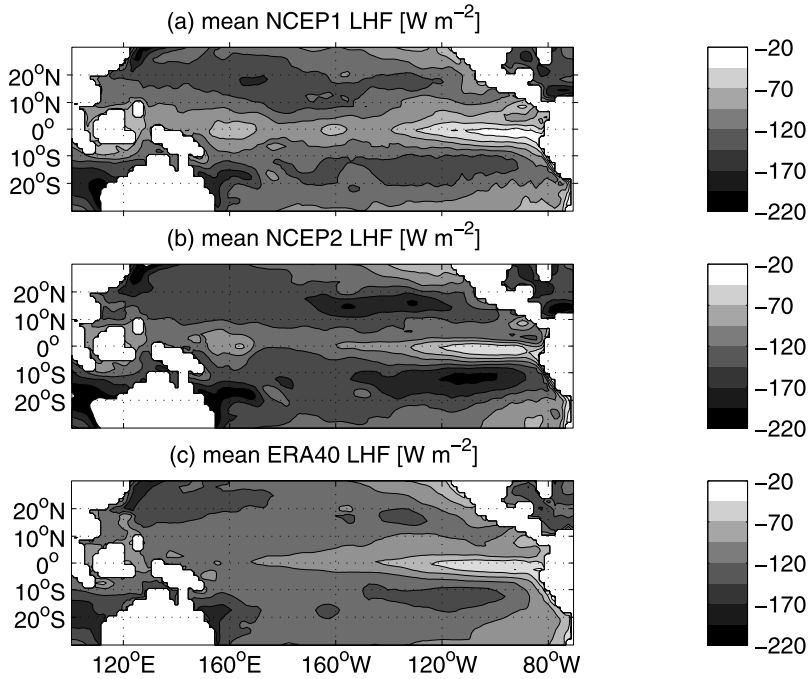

Figure 11. Two-year mean NWP LHF products in the tropical Pacific (30°S to 30°N): (a) NCEP1, (b) NCEP2, and (c) ERA40. Note the larger LHF in NCEP2 LHF off the equator.

[35] In this paper, surface state variables and a hybrid turbulent heat flux product estimated with the state-of-the-art COARE v3.0 algorithm using NWP reanalysis (NCEP1, NCEP2 and ERA40) variables and satellite retrievals (QuikSCAT winds and MW/OI SST) are compared with TAO buoy observations for 2000–2001 in the equatorial Pacific. In comparisons with TAO anemometer winds, QuikSCAT winds are shown to be more accurate and to produce a smaller latent heat flux RMS error than NWP winds. When averaged over 38 TAO buoys, the bias and standard deviation of difference (SDD) for QuikSCAT wind speed are 0.0 m s^{-1} and 0.5 m s^{-1}, respectively. Additionally, the bias and SDD of latent heat flux using the QuikSCAT wind speed are -4.0 W m^{-2} and 6.9 W m^{-2}. Microwave SST is desirable to estimate the LHF because of its high spatial resolution and all-weather capability; it has a lower SDD than other SST products, but a larger bias. The bias and SDD of LHF caused by MW/OI SST are 3.7 W m^{-2} and 8.5 W m^{-2}, again with a smaller SDD, but larger bias than other SST products. For surface air specific humidity and air temperature, ECMWF reanalysis ERA40 provides the best fields among three NWP reanalysis products. The bias and SDD of LHF caused by ERA40 air specific humidity are -4.8 W m^{-2} and 11.0 W m^{-2}. The error of LHF to the state variables shows that the accuracy of air specific humidity, wind speed, and SST are most important to the accuracy of LHF estimation.

[36] On the basis of these comparisons and the error analysis, we selected the ERA40 state variables to combine with QuikSCAT winds and microwave SST to create a fourth (hybrid) turbulent heat flux estimate using COARE v3.0 algorithm in the tropical Pacific (30°S to 30°N). The average (over 38 TAO buoy) bias and SDD of the hybrid latent heat flux are -5.8 W m^{-2} and 16.2 W m^{-2}, which is comparable to the accuracy of LHF derived from TAO measurements. The RMS error of the hybrid latent heat flux is comparable to that of ERA40 LHF estimated from COARE v3.0, but the hybrid products are expected to give better spatial resolution than NWP products.

[37] Comparisons of NWP turbulent heat fluxes estimated from COARE v3.0 to NWP reanalysis products at TAO buoys show that the COARE v3.0 algorithm and the reanalysis state variables together improved mean turbulent heat fluxes of NCEP2 and ERA40, reducing the NCEP2 latent heat flux bias from 28.6 W m^{-2} to 8.9 W m^{-2}. However, the NCEP1 reanalysis mean LHF bias (4.7 W m^{-2} high) is much smaller than the LHF estimated from the COARE v3.0 algorithm (10.7 W m^{-2} low), probably because of compensation for weak wind speeds in the NCEP1 bulk algorithm.

[38] Off the equator, the mean hybrid LHF is much higher than the NWP LHF estimates using the COARE v3.0 algorithm, which is probably owing to the combination of the low air specific humidity of ERA40, the strong wind speed of QuikSCAT, and the warm MW/OI SST. The structure of the hybrid LHF is very similar to that of NCEP1 reanalysis product.

[39] The net surface heat flux is the sum of the net solar radiation, net longwave radiation, and the turbulent heat fluxes. This paper has analyzed the errors in the turbulent heat fluxes for the tropical Pacific. Net solar radiation from NWP are also expected to produce significant errors to the net surface heat fluxes [e.g., *Josey*, 2001; *Wang and McPhaden*, 2001]. Evaluation of the NWP and satellite radiation fields against in situ data is beyond the scope of this paper. Ocean modelers who are interested in accurate turbulent heat fluxes in the tropical Pacific might find the hybrid products useful.

[40] **Acknowledgments.** The authors would like to acknowledge Suzanne Dickinson for preparing the QuikSCAT gridded wind speed field and NWP fields. NCEP reanalysis data are provided by the NOAA-CIRES Climate Diagnostics Center, Boulder, Colorado, USA, from their Web site at http://www.cdc.noaa.gov/. NCEP reanalysis daily state variables, such as sea surface temperature, 2-m air temperature, 2-m air specific humidity, and sea level pressure, are obtained from NCEP reanalysis Web sites at ftp://ftp.cdc.noaa.gov/Datasets/ncep.reanalysis.dailyavgs/ (NCEP1) and at ftp://ftp.cdc.noaa.gov/Datasets/ncep.reanalysis2.dailyavgs/ (NCEP2). NCEP reanalysis 6-hourly zonal and meridional wind vectors are taken from ftp://ftp.cdc.noaa.gov/Datasets/ncep.reanalysis/ (NCEP1) and ftp://ftp.cdc.noaa.gov/Datasets/ncep.reanalysis2/ (NCEP2). Four analyses per day from ECMWF ERA40 data used in this paper have been obtained from the ECMWF data server http://data.ecmwf.int/data/d/era40_daily/ (0000, 0600, 1200, and 1800 UTC). The TAO buoy data are from NOAA's Pacific Marine Environmental Laboratory (PMEL) (http://www.pmel.noaa.gov/tao/data_deliv/). We also acknowledge the TAO Project Office (Michael J. McPhaden, Director). Helpful comments from two anonymous reviewers are greatly appreciated. This work is supported by NASA's Ocean Vector Winds Science Team through contract 1216233 with the Jet Propulsion Laboratory. This is PMEL contribution 2770.

References

Bourassa, M. A. (2004), An improved sea state dependency for surface stress derived from in situ and remotely sensed winds, *Adv. Space Res.*, *33*(7), 1136–1142.

Bourassa, M. A. (2005), Satellite-based observations of surface turbulent stress during severe weather, in *Atmosphere-Ocean Interactions*, vol. 2, edited by W. Perrie, WIT Press, Ashurst, UK, in press.

Bourassa, M. A., D. M. Legler, J. J. O'Brien, and S. R. Smith (2003), SeaWinds validation with research vessels, *J. Geophys. Res.*, *108*(C2), 3019, doi:10.1029/2001JC001028.

Brunke, M. A., and X. Zeng (2002), Uncertainties in sea surface turbulent flux algorithms and data sets, *J. Geophys. Res.*, *107*(C10), 3141, doi:10.1029/2001JC000992.

Brunke, M. A., C. W. Fairall, X. Zeng, L. Eymard, and J. A. Curry (2003), Which bulk aerodynamic algorithms are least problematic in computing ocean surface turbulent fluxes?, *J. Clim.*, *16*, 619–635.

Chelton, D. B., S. K. Esbensen, M. G. Schlax, N. Thum, and M. H. Freilich (2001), Observations of coupling between surface wind stress and sea surface temperature in the eastern tropical Pacific, *J. Clim.*, *14*, 1479–1498.

Chou, S.-H., E. J. Nelkin, J. Ardizaone, R. M. Atlas, and C. L. Shie (2003), Surface turbulent heat and momentum fluxes over global oceans based on the Goddard Satellite Retrievals, version 2 (GSSTF2), *J. Clim.*, *16*, 3256–3273.

Clayson, C. A., and J. A. Curry (1996), Determination of surface turbulent fluxes for the Tropical Ocean-Global Atmosphere Coupled Ocean-Atmosphere Response Experiment: Comparison of satellite retrievals and in situ measurements, *J. Geophys. Res.*, *101*(C12), 28,515–28,528.

Contreras, R. F., and W. J. Plant (2004), Ku-band backscatter from the Cowlitz River: Bragg scattering with and without rain, *IEEE Trans Geosci. Remote Sens.*, *42*, 1444–1449.

Cronin, M. F., and M. J. McPhaden (1997), The upper ocean heat balance in the western equatorial Pacific warm pool during September-December 1992, *J. Geophys. Res.*, *102*(C4), 8533–8553.

Curry, J. A., et al. (2004), SEAFLUX, *Bull. Am. Meteorol. Soc.*, *85*, 409–424.

Fairall, C. W., E. F. Bradley, G. A. Godfrey, G. A. Wick, J. B. Edson, and G. S. Young (1996a), Cool-skin and warm-layer effects on sea surface temperature, *J. Geophys. Res.*, *101*(C1), 1295–1308.

Fairall, C. W., E. F. Bradley, D. P. Rogers, J. B. Edson, and G. S. Young (1996b), Bulk parameterization of air-sea fluxes for Tropical Ocean-Global Atmosphere Coupled-Ocean Atmosphere Response Experiment, *J. Geophys. Res.*, *101*(C2), 3747–3764.

Fairall, C. W., E. F. Bradley, J. E. Hare, A. A. Grachev, and J. B. Edson (2003), Bulk parameterization of air-sea fluxes: Updates and verification for the COARE algorithm, *J. Clim.*, *16*, 571–591.

Huddleston, J. N. (2000), Multidimensional histogram (MUDH) rain flag product description, version 2.1, Jet Propul. Lab., Pasadena, Calif.

Jones, C., P. Peterson, and C. Gautier (1999), A new method for deriving ocean surface specific humidity and air temperature: An artificial neutral network approach, *J. Appl. Meteorol.*, *38*, 1229–1245.

Josey, S. A. (2001), A comparison of ECMWF, NCEP-NCAR, and SOC surface heat fluxes with moored buoy measurements in the subduction region of the northeast Atlantic, *J. Clim.*, *14*, 1780–1789.

Kalnay, E., et al. (1996), The NCEP/NCAR 40-year Reanalysis Project, *Bull. Am. Meteorol. Soc.*, *77*, 437–471.

Kanamitsu, M., W. Ebisuzaki, J. Woolen, J. Potter, and M. Fiorion (2000), An overview of NCEP/DOE Reanalysis-2, paper presented at 2nd International Conference on Reanalyses, Mt. Washington Obs., Reading, UK.

Kelly, K. A., S. Dickinson, and Z.-J. Yu (1999), NSCAT tropical wind stress maps: Implications for improving ocean modeling, *J. Geophys. Res.*, *104*(C5), 11,291–11,310.

Kelly, K. A., S. Dickinson, M. J. McPhaden, and G. C. Johnson (2001), Ocean currents evident in satellite wind data, *Geophys. Res. Lett.*, *28*(12), 2469–2472.

Kelly, K. A., S. Dickinson, and G. C. Johnson (2005), Comparisons of scatterometer and TAO winds reveal time-varying surface currents for the tropical Pacific Ocean, *J. Atmos. Oceanic Technol.*, *22*, 735–745.

Klinker, E. (1997), Diagnosis of the ECMWF model performance over the tropical oceans, in *Proceedings of Seminar on Atmosphere-Surface Interaction*, pp. 53–66, Eur. Cent. for Medium-Range Weather Forecasts, Reading, UK.

Liu, W. T., K. B. Katsaros, and J. A. Businger (1979), Bulk parameterizations of air-sea exchanges of heat and water vapor including molecular constraints at the interface, *J. Atmos. Sci.*, *36*, 1722–1735.

Mears, C. F. (2000), SeaWinds on QuikSCAT normalized objective function rain flag, version 1.2, 13 pp., Remote Sens. Syst., Santa Rosa, Calif.

Schlax, M. D., D. B. Chelton, and M. H. Freilich (2001), Sampling errors in wind fields constructed from single and tandem scatterometer data sets, *J. Atmos. Oceanic. Technol.*, *10*, 1014–1036.

Smith, A. D. (1988), Coefficients for sea surface wind stress, heat flux, and wind profiles as a function of wind speed and temperature, *J. Geophys. Res.*, *93*(C12), 15,467–15,472.

Smith, S., D. M. Legler, and K. V. Verzone (2001), Quantifying uncertainties in NCEP reanalysis using high-quality research vessel observations, *J. Clim.*, *14*, 4062–4072.

Stiles, B. W. (2002), Impact of rain on spaceborne Ku-band wind scatterometer data, *IEEE Trans. Geosci. Remote Sens.*, *40*, 1973–1983.

Sun, B., L. Yu, and R. A. Weller (2003), Comparisons of surface meteorology and turbulent heat fluxes over the Atlantic: NWP model analyses versus moored buoy observations, *J. Clim.*, *16*, 679–695.

Tournadre, J. (2003), Impact of rain cell on scatterometer data: 1. Theory and modeling, *J. Geophys. Res.*, *108*(C7), 3225, doi:10.1029/2002JC001428.

Wang, W., and M. J. McPhaden (2001), What is the mean seasonal cycle of surface heat flux in the equatorial Pacific, *J. Geophys. Res.*, *106*(C1), 837–857.

Yu, L., R. A. Weller, and B. Sun (2004), Mean and variability of the WHOI daily latent and sensible heat fluxes at in situ flux measurement sites in the Atlantic Ocean, *J. Clim.*, *17*, 2096–2118.

M. F. Cronin, NOAA Pacific Marine Environmental Laboratory, 7600 Sand Point Way NE, Seattle, WA 98115, USA.

C. Jiang and L. Thompson, School of Oceanography, University of Washington, Box 357940, Seattle, WA 98195, USA. (chuanlij@ocean.washington.edu)

K. A. Kelly, Applied Physics Laboratory, University of Washington, 1013 NE 40th Street, Box 355640, Seattle, WA 98105-6698, USA.